

Investigation into Crack Phenomena of Unreinforced Concrete Structures for Aseismic Evaluation of Concrete Dams

by

Tadahiko Sakamoto¹, Yoshikazu Yamaguchi², Takashi Sasaki³, Kei Takafuji⁴, Ken-ichi Kanenawa⁵

ABSTRACT

We have conducted research on non-linear analysis for concrete dams using the smeared crack model. Efforts to verify applicability and accuracy of such numerical analyses for concrete dams have been made through simulations for actual damages of existing concrete dams due to large earthquakes. But, a more quantitative evaluation of the cracking process of concrete dams using crack analysis is needed in order to use such analytical method to estimate the limit state of concrete dams against large earthquakes.

In the present study, we conducted shaking table tests on pillar-shaped unreinforced concrete specimens to investigate the effect of cracks on the dynamic behavior of concrete structures. The results showed that as tensile fracture progresses, the first resonant frequency of the specimen lowers and the damping increases. We simulated vibration tests by non-linear dynamic analysis based on the smeared crack model. Based on a comparison of the test results and numerical simulation, we discuss how to set parameters for numerical simulation such as the tension softening curve and damping ratio, to simulate the cracking behavior of unreinforced concrete structures such as concrete dams.

KEYWORDS: Non-linear FEM Analysis, Shaking Table Test, Smeared Crack Model, Tensile Fracture, Unreinforced Concrete Structure.

1. INTRODUCTION

As a consequence of frequent large earthquakes that have occurred in Japan in recent years, evaluating the seismic safety of various infrastructures has become an important and urgent issue. In this situation, the Ministry of Land, Infrastructure and Transport of the Japanese Government published the “*Guidelines for Seismic Performance Evaluation of Dams (Draft)*” [1] in March 2005.

According to the guidelines, numerical analysis considering the tensile fracture of concrete is needed to evaluate the seismic safety of concrete gravity dams in the event of a large earthquake. The authors have considered the seismic safety of concrete gravity dams by performing non-linear analysis using a smeared crack model [2]. However, the applicability of these kinds of analysis methods has only been confirmed in a qualitative manner based on a comparison with limited cases of cracking of existing dams [3]. Therefore, there is a need to quantitatively evaluate the occurrence and propagation phenomena of cracking caused by the dynamic load in order to accurately evaluate the seismic safety of dams. Examples of research conducted to develop this type of quantitative evaluation are studies by Tinawi et al. [4], Uruchida et al. [5] and Kashiwayanagi et al. [6], who performed vibration

¹ Chief Executive, Public Works Research Institute (PWRI), Tsukuba-shi, Ibaraki-ken 305-8516 Japan.

² Team Leader, Dam Structure Research Team, Hydraulic Engineering Research Group, ditto.

³ Senior Researcher, ditto.

⁴ Collaborating Researcher, ditto.

⁵ Chief Official, River Planning Division, River Bureau, Ministry of Land, Infrastructure and Transport (MLIT), Chiyoda-ku Tokyo-to 100-8918 Japan.

testing of concrete gravity dam models. This paper reports a study about vibration fracture of unreinforced concrete using pillar-shaped models made of low-strength concrete [7]. The results revealed the influence of tensile cracking of the concrete on the first resonant frequency and the damping ratio of the test model. A numerical analysis was attempted in order to simulate cracking in the test models by finite element analysis using the smeared crack model.

2. SHAKING TABLE TESTS

2.1 Experimental Method

2.1.1 Material Composition for Test Model

The test material used was low-strength concrete so that the vibration testing would cause tensile fractures. The concrete mix proportion conditions and the materials used are shown in Table 1. The maximum aggregate size was set at 20 mm so that the test materials would have a certain degree of fracture energy.

Table 1 Test model materials: Mix conditions and materials used

Water : cement ratio	330 %
Max. aggregate size	20 mm
Cement	Moderate heat Portland cement
	67 kg/m ³
Admixture	Limestone powder
	433 kg/m ³

2.1.2 Shape of Test Model

The shape of the test model was decided as shown in Fig. 1(a), taking into account the following conditions: (1) the first resonant frequency of the test model is within the range of the excitation capacity of the shaking table which is planned to be used and (2) it is possible to roughly specify the location where tensile cracking will occur. In order to control the first resonant frequency, a

weight of 100 kg was applied to the top of the test model. Excitation was applied using a white noise waveform with maximum acceleration amplitude of about 30 gal, to calculate the resonance curve shown in Fig. 1(b). As a result, the first resonant frequency of the test model before fracturing was about 30 Hz.

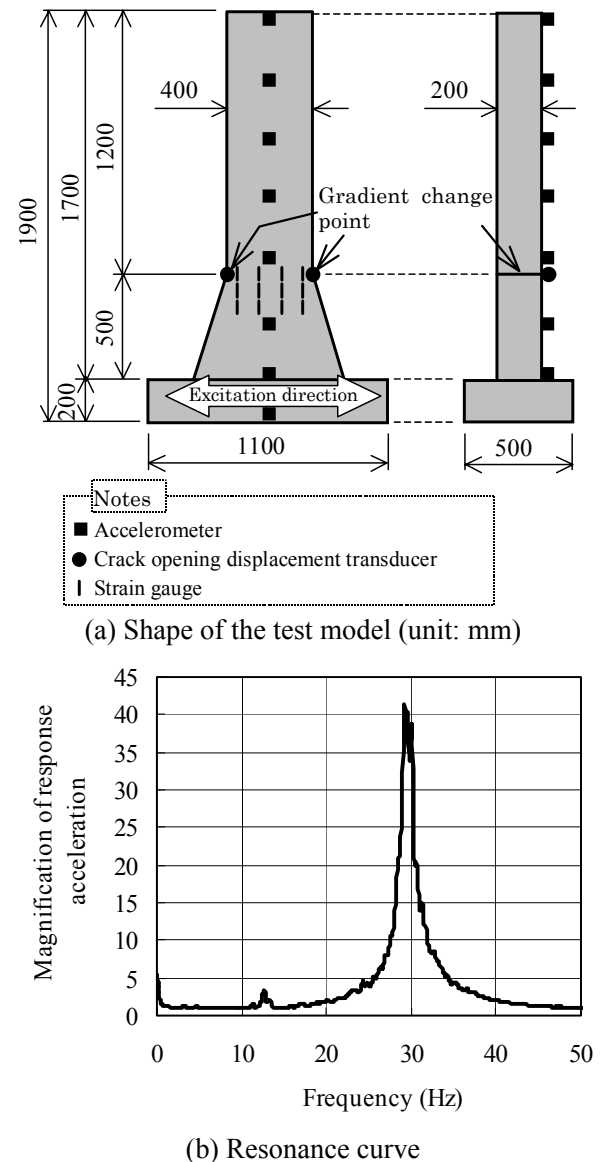


Fig. 1 Test model shape and resonance curve

2.1.3 Measurement Instruments

On the test model, accelerometers, crack opening displacement transducers and strain gauges were installed. The sampling interval was about 0.001 second (1,000 Hz). The layout of the major instruments is shown in Fig. 1(a). Visual observation was conducted using a high-speed video camera.

2.1.4 Input Acceleration Wave

The input wave was set as a sinusoidal wave of 22 Hz. In the case of excitation frequency of 22 Hz, the acceleration response multiplier at the top of the test model is expected to be about 2.5 times from Fig. 1(b). To make it possible to sufficiently observe the steady response of the test model in one excitation, the excitation time was set to 2 seconds. The amplitude was gradually increased at the beginning period of each excitation. The acceleration amplitude was set to be constant in one excitation, and it was increased step by step with the progress of excitation cases.

2.1.5 Material Properties of Test Model

Table 2 shows the material properties of the test model obtained by laboratory testing.

To obtain the tensile softening properties of the material, a wedge penetration type splitting test was performed in compliance with AAC13.1 of RILEM [8]. The specimen was a rectangular parallelepiped with width of 200 mm, height of 1700 mm and thickness of 100mm shown in Fig. 2. Fig. 3 shows the tensile softening curve estimated by a program provided by JCI [9] based on back analysis method by using the results of load – crack opening displacement results obtained by the wedge penetration type splitting test. And, approximated bilinear softening curve is shown in this Figure. This approximation was estimated so that it is possible to accurately reproduce the results of the wedge penetration type splitting test by FEM numerical analysis. The stress f_t at the start of tensile softening of the bilinearly approximated tensile softening curve was 0.23 MPa and the fracture energy G_f was 10.5 N/m.

Table 2 Material properties

Property	Value
Compressive strength	1.85 MPa
Splitting tensile strength	0.17 MPa
Elastic modulus	5,260 MPa
Unit weight	2.3 t/m ³
Poisson's ratio	0.15

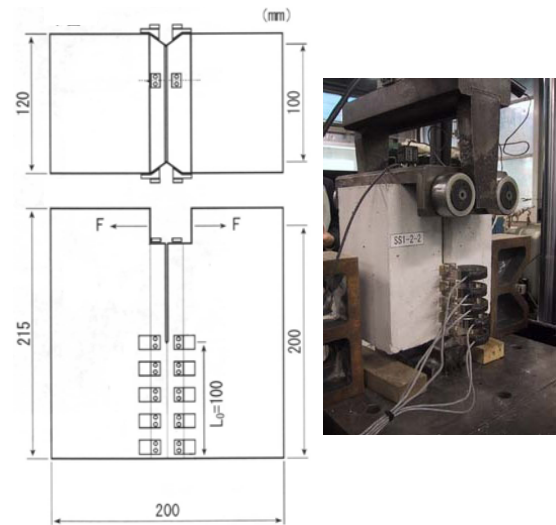


Fig. 2 Wedge penetration type splitting test

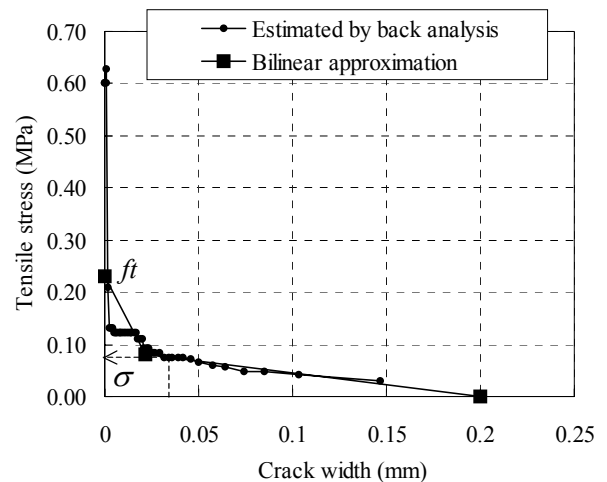


Fig. 3 Tensile softening curve obtained by the wedge penetration type splitting test

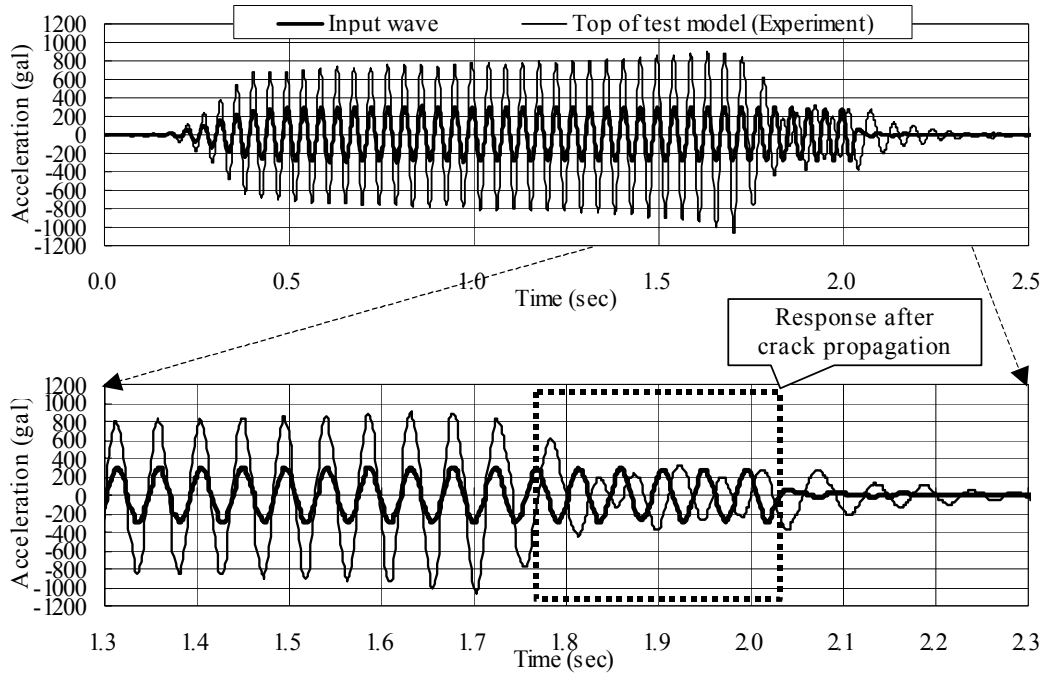


Fig. 4 Response acceleration at top of test model (Input acceleration 300 gal)

2.1.6 Response Acceleration of Top of Test Model
 Fig. 4 shows the input acceleration and the response acceleration at the top of the test model in the case with input acceleration of 300 gal. The response at the top of the test model is shown to be steady-state vibration with identical phase to the input acceleration from 0.5 until about 1.5 seconds, but from about 1.7 seconds, the response acceleration amplitude falls sharply. This is presumed to be a result of a crack propagating in the test model and passing through it at the 1.7-second point. This was confirmed by the results of comparison analysis between crack width defined in 2.1.7 and picture data by high-speed video camera. A phase difference of about 160° was observed between the top response acceleration and the input acceleration after the crack passed through the test model.

2.1.7 Degree of Tensile Fracture

The degree of tensile fracture was defined by Eq. 1 in order to quantitatively evaluate the degree of

tensile fracture of the test model. At the time when the degree of tensile fracture was 100%, the tensile softening state had ended and there was a completely opened tensile crack.

$$[\text{Degree of tensile fracture (\%)}] = (f_t - \sigma) \times 100 / f_t \quad (1)$$

where, f_t represents the stress at the start of tensile softening (0.23 MPa) and σ represents the tensile stress (tensile stress at crack surface) which corresponds to the crack opening displacement in Fig. 3. The crack width that was used here was calculated by subtracting the maximum elastic deformation from the measured crack opening displacement at the gradient change point shown in Fig. 1. The maximum elastic deformation Δx is obtained by the following equation.

$$\Delta x = f_t \times l / E = 0.0044 \text{ mm},$$

where, Δx : maximum displacement in the elastic range, f_t : stress at the start of tensile softening, E : elastic modulus, l : marked point interval between opening displacement gauges (100 mm).

Table 3 Degree of tensile fracture

Input acceleration amplitude (gal)	Crack opening displacement (mm)	Crack width (mm)	Tensile stress at crack surface (MPa)	Degree of tensile fracture (%)
30	0.0018	0.0000	—	0.0
150	0.0075	0.0031	0.209	9.3
300	0.0600	0.0556	0.065	72.0
900	0.1600	0.1556	0.020	91.3

In the test case with input acceleration amplitude of 30 gal, the crack opening displacement was set at 0.0 m because the measured crack displacement was not exceed the maximum displacement within the elastic range.

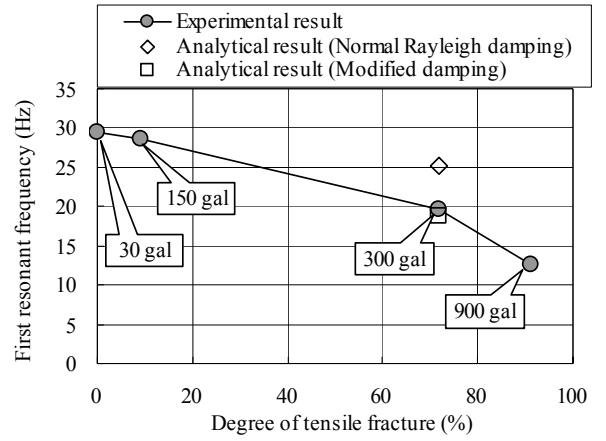
Table 3 shows the degree of tensile fracture in each test case calculated based on the crack width during steady state vibration. The crack width was calculated from the measured value by the crack opening displacement inducer, and the tensile stress at crack surface was evaluated the correspond value to the crack opening displacement on the bilinear approximation line in Fig. 2. In the test case with input acceleration amplitude of 30 gal, tensile cracking did not occur, and in the 150 gal case, tensile stress just over the tensile strength of material was produced and tensile fracturing occurred, although only to a small degree.

2.1.8 Relationship between First Resonant Frequency and Degree of Tensile Fracture

Fig. 5 shows the relationship of the degree of tensile fracture with the first resonant frequency calculated based on the response acceleration in the free vibration immediately after termination of the excitation. The open symbol plots in Fig. 5 and Fig. 6 show the analysis results discussed below. This reveals that as the fracture progresses, the first resonant frequency falls.

In the case with input acceleration amplitude of 150 gal, there is almost no decline of the first resonant frequency from 30 Hz prior to fracturing. On the other hand, in the 300 gal case, the first resonant frequency falls to about 20 Hz, which is

lower than the frequency of the input waves (22Hz). This presumably caused the phase difference shown in Fig. 4.



Note: numbers in the figure are the input acceleration amplitude.

Fig. 5 Relationship of the degree of tensile fracture with the first resonant frequency

2.1.9 Relationship between Damping Ratio and Degree of Tensile Fracture

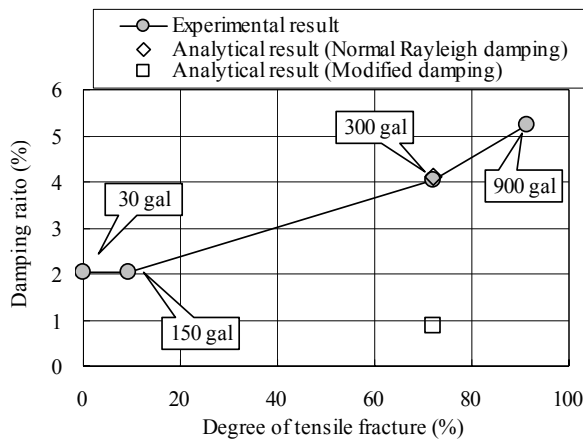
Fig. 6 shows the relationship of the degree of tensile fracture with the apparent damping ratio obtained based on the response acceleration in the free vibration. The damping ratio was calculated as the average value when $m = 1$ to 4, and $n = 3$ based on Eq. 2.

$$|y_m / y_{m+n}| = \left(e^{2\pi h / \sqrt{1-h^2}} \right)^n \quad (2)$$

where, y_m and y_{m+n} represent the m and $(m+n)$ th amplitude respectively, and h represents the

damping ratio.

Fig. 6 reveals that as the degree of tensile fracture increases, the apparent damping ratio rises. In a vibration fracture test of a concrete gravity dam model performed by Tinawi et al., it was reported that the occurrence of a crack tended to increase the damping ratio [3]. It is hypothesized that on the fracture surface where the crack occurred, the impact of the re-closing of the crack induces a local fine fracture, which consumes energy. This would result in an increase in the apparent damping ratio accompanying the appearance of the crack.



Note: numbers in the figure are the input acceleration amplitude.

Fig. 6 Relationship of the degree of tensile fracture with the damping ratio

3. NUMERICAL SIMULATION WITH NON-LINEAR FINITE ELEMENT METHOD

3.1 Numerical Analysis Method

Non-linear finite element analysis based on the smeared crack model was carried out to reproduce the results of the vibration testing.

The analysis was two-dimensional hypothesizing the plane stress state, and the concrete tensile softening phenomenon was represented by the bilinear tensile softening curve shown in Fig. 3. The damping matrix in the equation of motion was

set by hypothesizing Rayleigh damping at a damping ratio of 2% based on the first and second resonant frequencies. The damping ratio was set so that it would be possible to simulate the behavior of the test model before fracturing. The bottom of the test model was considered to be a fixed boundary in FEM analyses.

3.2 Material Properties for Numerical Analysis

The material properties used for the analysis were set and based on the results of laboratory testing, excluding the elastic modulus E , as shown in Table 4. To make the first resonant frequency of the test model evaluated by the analysis correspond with the value observed in the test, the elastic modulus E was set at 6,500 MPa, which is a little higher than that evaluated by the material tests.

Table 4 Material properties for numerical analysis

Material property	Notation	Value
Elastic modulus	E	6,500 MPa
Poisson's ratio	ν	0.15
Unit weight	γ	2.3 t/m ³
Damping ratio	h	2%

3.3 Analytical Results

In the numerical analysis, the crack in the test model was almost passed through the test model in the case with input acceleration amplitude of 340 gal. On the other hand, in the vibration test, the crack passed through at 300 gal. This is presumably due to the fact that the stress at the start of tensile softening f_t of the bilinearly approximated tensile softening curve in Fig.2 was about 35% larger than the splitting tensile strength of the test material. The analysis results conform closely to the test results in terms of the crack location.

Fig. 7 shows the response acceleration time history at the top of the test model obtained by analysis.

The following description focuses on the response after 1.0 second when the crack had almost passed

through the test model. The phase difference of the top response acceleration to the input wave was calculated to be about only 80° . In the test, on the other hand, a phase difference of about 160° was caused, which is a very different value. Focusing on the reduction of the response acceleration amplitude after the crack passed through, the analysis found no rapid decline of the response acceleration amplitude after the crack passed through as observed by the test. One cause of this phenomenon was an over-evaluation of the viscous damping force in elements in which crack occurred. After a crack occurs, the damping force should not be transmitted passing the crack surface. The decline of the viscous damping force accompanying the occurrence of a crack is not considered by normal Rayleigh damping with smeared crack model.

In order to appropriately represent the reduction of the viscous damping force on the crack surface, reducing the damping force according to the state of the propagation of the crack was proposed by Bhattacharjee and Léger [10], and Kimata et al. [11]. In the present study, non-linear analysis with damping matrix which depends on the state of stiffness matrix with taking consideration of crack was performed. It is similar to methods which were used in abovementioned researches. The damping matrix was set to be consisted from only stiffness matrix, different from Rayleigh damping. In the following study, we call this damping “modified damping”.

Fig. 8 shows the results of the analysis based on modified damping. Focusing on the response acceleration before cracking, from 0.5 second to about 1.0 second does not show a clear difference between the analysis using normal Rayleigh damping and the analysis with modified damping. This reveals that there are not so large differences between modified damping and Rayleigh damping on the response properties until the crack almost penetrate the test model. Next, focusing on the top response beginning at about 1.0 second when the cracking had propagated reveals large differences between the results in Fig. 7 and Fig. 8. Using the

method with modified damping, the phase difference between the input acceleration and the response acceleration at the top of the model was about 160° . This result conforms closely to the vibration test result. The analysis also represented the abrupt decline of the response acceleration amplitude after cracking. It can be seen that modified damping can more appropriately reproduce the response after propagation of the crack.

In Fig. 5 and Fig. 6, the first resonant frequency and the damping ratio obtained by numerical analyses in the case with input acceleration of 340 gal are also shown. Degree of tensile fracture of these data was equalized with result of vibration test in case of input acceleration of 300 gal. According to these figures, in the analysis with modified damping, although the first resonant frequency conformed closely to the test result, the damping ratio was lower than the test result. This is considered to be because the rise of the apparent damping accompanying the propagation of tensile fracture observed in the test was not considered in the numerical analysis.

There was also a little difference between the absolute values of the response acceleration amplitude after cracking obtained by analysis and by the vibration test. For these phenomena, it is necessary to study the damping ratio for the overall system according to the degree of progress of cracking (change of the resonant frequency of the overall structure by cracking).

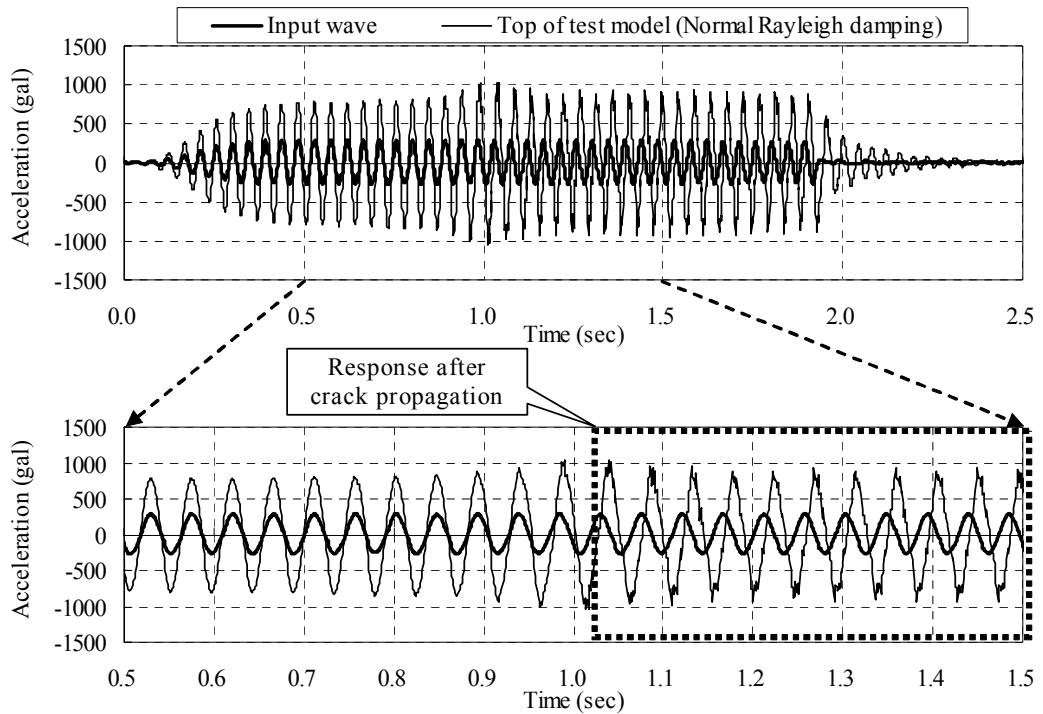


Fig. 7 Acceleration response at top of test model (Normal Rayleigh damping)

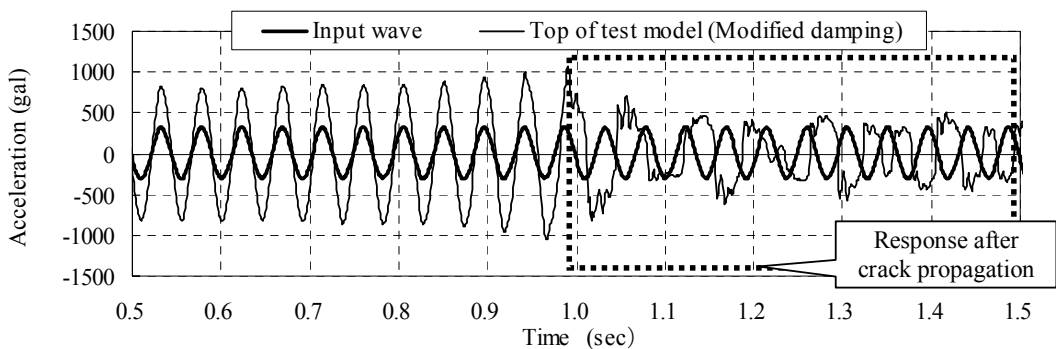


Fig. 8 Acceleration response at top of test model (Modified damping)

4. CONCLUSIONS

This research examined the performance of vibration fracture testing using a pillar-shaped test model made of low-strength concrete to investigate numerical analysis for aseismic evaluation of concrete dams. The following

conclusions were drawn.

- This vibration test confirmed that the progress of tensile fracture was accompanied by a decline of the first resonant frequency and an increase in the apparent damping ratio.
- In the results of the analysis using the tensile softening curve, the location of the crack

conformed closely with that in the vibration test results.

- In the case of analysis using Rayleigh damping, the phase and amplitude of the response acceleration after the crack nearly penetrated were greatly different from those in the vibration test results.
- In the analysis with modified damping which damping matrix depend on state of stiffness matrix, the response acceleration at the top of the test model obtained by the analysis and that of the vibration test conformed closely.

A future challenge is to use the results of this research to propose a method of setting material properties including damping ratio for accurately evaluating the seismic safety of a concrete gravity dam. The authors have conducted a vibration fracture test using a large-scale model and simulation analyses for the vibration test, so we'd like to report those results in the near future.

5. REFERENCES

1. River Bureau, Ministry of Land, Infrastructure and Transport: *Guideline for Seismic Performance Evaluation of Dams (Draft)*, 2005.3. (in Japanese)
2. Sasaki, T., Kanenawa, K., Yamaguchi, Y. and Chiba, J.: Effect of ground motion level and dam shape on damage in concrete gravity dam during earthquakes, *Proceedings of 73rd Annual Meeting of ICOLD*, 2005.5.
3. for example, Zhang, H. and Ohmachi, T. 2 dimensional analysis of seismic cracking in concrete gravity dams, *Journal of Japan Society of Dam Engineers*, Vol.8, No.2, pp. 93-101, 1998.6
4. Tinawi, R., Léger, P., Leclerc. M. and Cipolla, G.: Seismic safety of gravity dams: From shake table experiments to numerical analyses, *Journal of Structural Engineering*, pp. 518-529, 2000.4.
5. Uruchida, S., Shimpō, T., Uchida, Y., Yagome, Y. and Saouma, V.: Dynamic centrifuge tests of concrete gravity dam, *Proceedings of 73rd Annual Meeting of ICOLD*, 2005.5.
6. Kashiwayanagi, M., Horii, H., Nakayama, Y. and Asaka, H.: Evaluation on crack propagation analysis for earthquake resistance assessment of gravity dams, *Proceedings of 73rd Annual Meeting of ICOLD*, 2005.5.
7. Sasaki, T., Takafuji, K., Yamaguchi, Y., Kanenawa, K. and Ishibashi, M.: Effect of Cracks on Dynamic Behavior Characteristics of Unreinforced Concrete Structures, *Proc. of 8th National Conference on Earthquake Engineering*, 2006.4.
8. RILEM AAC13.1: Determination of the specific fracture energy and strain softening of AAC, *RILEM Technical Recommendations for the Testing and Use of Construction Materials*, pp.156-158, 1994.
9. Japan Concrete Institute: Method of test for fracture energy of concrete by use of notched beam, *JCI-S-001-2003*, 2003. (in Japanese)
10. Bhattacharjee, S. S. and Léger, P.: Seismic cracking and energy dissipation in concrete gravity dams, *Earthquake Engineering and Structural Dynamics*, Vol.22, pp. 991-1007, 1993.
11. Kimata, H., Fujita, Y., Niimi, K., Hoshido, T., Kase, T., Hikawa, N. and Horii, H.: Seismic safety of concrete gravity dams based on dynamic crack propagation analysis during large-scale earthquakes, *Proceedings of 73rd Annual Meeting of ICOLD*, 2005.5.